Modeling Fluid Mixing in Microfluidic Grids

Huong Luu
Department of Computer Science
University of California at Riverside

Marek Chrobak
Department of Computer Science
University of California at Riverside

Abstract

We describe an approach for modeling fluid concentration profiles in grid-based microfluidic chips for fluid mixing. This approach provides an algorithm that predicts fluid concentrations at the chip outlets. Our algorithm significantly outperforms COMSOL finite element simulations in term of runtime while still produces results that closely approximate those of COMSOL.

1 Introduction

Microfluidics is an emerging technology for manipulating nanoliter-scale fluid volumes, with applications in a variety of fields including biology, chemistry, biomedicine, and materials science. Fast progress in this area led to the development of microfluidic chips (MFCs), which are integrated microfluidic devices that are increasingly often used in various laboratory processes such as medical diagnosis [15], DNA purification [9], or cell lysis [8]. MFCs offer a solution to automate laboratory experiments that saves time, reduces labor costs, limits usage of chemical reagents, and replaces complex and expensive equipments [12, 8].

One function often implemented on MFCs is fluid mixing. The technologies for mixing MFCs currently in use fall into two broad categories: droplet-based chips, where the fluid is manipulated in discrete units called droplets, and flow-based chips, based on continuous flow. In this work we focus exclusively on the flow-based model.

Fluid mixing is particularly important in sample preparation, where the objective is to dilute the sample fluid, also called *reactant*, using another fluid that we refer to as *buffer*. For example, in cell lysis, the sample preparation process includes a step of mixing blood sample with citrate buffer [8]. For some experimental processes samples with multiple pre-specified volumes and concentrations are needed. For instance, such a sample may consist of $5\mu L$ of reactant with concentration 10%, $10\mu L$ of reactant with concentration 20%, and $10\mu L$ of reactant with concentration 40%. Samples involving such multiple target concentrations are common in preclinical drug development processes, and they are also used for other experiments, for example in biochemical assays [3]. For these applications, one needs to design a MFC that produces the specified target set of concentration/volume pairs of reactant.

Several flow-based designs have been proposed in the literature. In [11], the authors proposed an MFC that uses two-way valves to produce serial dilution. An electrokinetically driven MFC design was introduced in [6] for serial mixing. The above approaches require

different designs by changing valves or splitter channels placement, or tuning voltage control to create different target sets. In [4], the authors gave a dilution algorithm for given target concentration ratios using rotary mixers. However, their method produces waste, and it also uses valves which can complicate the fabrication process.

Grid mixers. A very different approach was developed by Wang *et al.* [14]. Their proposed solution involves creating a library of ready-to-use micromixers that users can query to find chip designs with desired properties. Their MFCs are simple rectilinear grids with two inputs (one for reactant and one for buffer) and three outputs, thus capable of producing a set of three different concentrations. They do not require any valves nor any other functional elements. A user identifies an appropriate design by submitting a query consisting of the desired reactant concentrations. In their approach the design process is eliminated and the database is created by exploring a large collection of randomly generated grids. For each random grid, its outlet concentration values are computed by simulating fluid flow through the grid using COMSOL Multiphysics® software (a commercial software that uses finite element analysis method to model physics processes, including fluid dynamics). As shown in [14], these COMSOL simulation results provide very accurate prediction of outlet concentrations in actual fabricated MFCs.

Exploring such random designs is extremely time consuming, as most randomly generated designs are actually not useful, either because they are redundant or because they produce concentrations that are of little interest (say, only near-pure reactant or buffer). Thus to produce a desired number of designs for the grid library, one may need to examine many orders of magnitude more random designs. Indeed, in our experiment, to produce a collection of 2600 sufficiently different concentration triplets we needed to generate 50 millions 12×12 random grid designs.

With the need to test so many designs, this approach can only be used for small size grids because of the simulation bottleneck of COMSOL Multiphysics®. The simulation time for each design in [14] is roughly a minute. It is also not scalable to bigger grids. COMSOL Multiphysics® takes about 6 minutes to run a simulation for a 12×12 grid with the same mesh setting. The process can be sped up by using a coarser mesh, but this results in degraded accuracy of concentration predictions at the outlets. Further, some users may prefer to design custom grids for their choices of the attributes: velocity, solute, outlets' locations, diffusion coefficient of reactant, etc. Such users would need to have access to an often costly computational fluid dynamics software in order to be able to run the simulations.

The approach based on random grid generation was also considered in [7], where the authors propose a method to remove redundant channels to make the design process more efficient, simplifying fabrication of grid MFCs and reducing reactant usage.

Our contribution. Addressing this performance bottleneck in populating the grid library in the approach from [14], we developed an algorithm to model fluid mixing in microfluidic grids, in order to predict the reactant concentrations at the outlets. In our approach, concentration profiles in grid channels are approximated using a simple 3-piece linear function, which allows us to simulate the mixing process in time linear in the grid size. The overall algorithm is scalable, simple, and produces good approximation of concentration values and flow rates at outlets in grid-based microfluidic chips, as compared to the results from COMSOL Multiphysics®. It is also much more general than the model from [14, 7], as it allows grids of all sizes, any number of outlets, arbitrary inflow velocities, and arbitrary fluids. We also developed a web-based implementation of our algorithm that allows users to customize
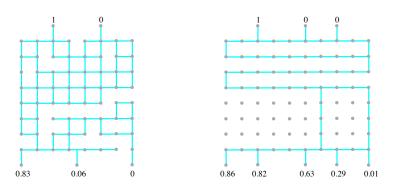
Figure 1 On the left, an example of an 8x8 grid from [14]. On the right, an example of a 10x8 grid in our model, with 3 inlets and 5 outlets. The numbers at the outlets show the reactant concentrations.

their designs manually to match their needs[1].

We add that our algorithm is not meant to be a complete substitute for COMSOL simulation. In the application to populating mixing grid libraries, as in [14], the recommended process would be to apply our algorithm to select a collection of randomly generated designs with potentially useful concentration vectors, and then re-verify these designs with COMSOL. This way, COMSOL simulation will be performed only on a tiny fraction of generated grids — less than %.01, according to our experiments. This significantly improves the overall performance.

While the main objective of this work was to develop an efficient numerical simulation algorithm, it also involves interesting combinatorial and topological aspects, as the correctness of our profile concentration model relies critically on duality properties of planar acyclic digraphs.

2   Statement of the Problem

We study grid-based MFCs for fluid mixing introduced in [14]. Their model is 8×8 grid with 2 inlets along the top edge of the grid and 3 outlets at the bottom, as shown in Figure 1. The left inlet contains reactant, with concentration value 1, and the right inlet contains buffer, with concentration value 0. The channel width is 0.2 mm, and the channel length (distance between two grid vertices) is 1.5 mm. The fluid velocity in the inlets is 10 mm/s. The outlets' pressure is 0 Pa. The reactant is either sodium, fluorescein or bovine serum albumin.

We generalize the model from [14] in several ways. We allow arbitrary $m \times n$ grids, with any number of inlets and outlets (see Figure 1). The inlets are located along the top edge of the grid and the outlets at the bottom. The inlets' solutions can take any concentration from 0 to 1, but they must satisfy the following *inlet monotonicity property*: the inlet concentrations need to be non-increasing from left to right. The inflows are of given constant rate, and the pressure values at all outlets are 0. Our model assumes that the flow throughout the grid is laminar, which is the case in standard microfluidic applications.

In this setting, the problem we address can be formulated as follows: We are given (1) the specification of a grid design, and (2) fluid properties, namely its concentration and velocity

---

[1] A prototype of this implementation is available at `http://algorithms.cs.ucr.edu`.

at each inlet and its diffusion coefficient. The goal is to determine the fluid concentration and velocity values at the outlets.

3   Overview of the Algorithm

Our algorithm for predicting reactant concentrations at the outlets is based on modeling its concentration profiles in grid's channels. Such a concentration profile is a function that represents concentration values of the reactant along a line perpendicular to the channel. When fluid flows through straight segments of the grid, this profile changes according to the laws of diffusion. In a node of the grid, a flow may be split or several flows may be joined, and the profile changes accordingly, producing complex non-linear functions. The main idea behind our algorithm is to approximate this profile using a simple 3-piece linear function. Once the profile at an output channel is computed, it determines the reactant concentration at this outlet.

We now give an overview of our algorithm, with more detailed descriptions given in the sections that follow.

(1) Verify the correctness of the grid design, namely whether each edge (channel) is on at least one inlet-to-outlet path. (In our implementation, spurious fragments of the grid are automatically removed.)

(2) Compute the flow rates in each channel and pressure values at each node (see Section 5).

(3) Partition the grid into parts, each part being either a straight channel or a node. Depending on flow direction, a node can be one of three types: a join node (2-way or 3-way), a split node (2-way or 3-way), or a combined join/split node (with 2 inflows and 2 outflows). Sort these parts in an order consistent with the flow direction. (Once the flows are computed, one can think of the grid design as an acyclic directed graph. The desired order is then any topological sort of this acyclic graph.)

(4) Process the grid parts, in the earlier determined order, computing approximate concentration profiles (see Section 6):

- For straight channels, the concentration profile at the end of the channel is determined from the profile at the beginning of the channel, based on the time the flow spends in this channel. This time is computed from the channel length and flow velocity.
- For nodes representing flow splits, split the incoming profile into outgoing profiles according to flow velocity ratios.
- For nodes representing flow joins, join the incoming profiles into the outgoing profile according to velocity ratios. This outgoing profile is then approximated by a 3-piece linear function.

(5) Once all flow profiles in the grid are determined, for each outlet compute its fluid concentration as the integral of its concentration profile divided by the channel width.

Running time. The algorithm for profile computations takes only constant time to update the profile for each node and channel, thus the overall running time is linear with respect to the size of the grid design. (Thus never worse than $O(mn)$ for an $m \times n$ grid.) The overall running time is dominated by solving the linear system in part (2). For grid sizes that might be of use in grid libraries, say up to 20×20, Gaussian elimination is sufficiently fast. For larger grids, one can take advantage of the sparsity of the linear system to speed up the computation.
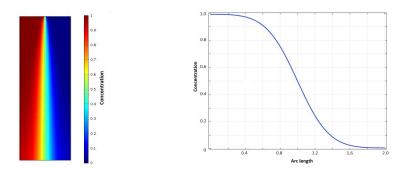
■ **Figure 2** The picture on the left shows the result of mixing of reactant (red) and buffer (blue) due to diffusion over some period of time. The figure on the right is a graph representing the concentration profile of this mixture at the end of the channel.

4 Concentration Profile Model

True concentration profiles. Consider a mixture of two fluids, one reactant (with concentration 1) and the other buffer (with concentration 0), flowing along a straight channel of some width w and length l. For any distance $l' \leq l$ from the beginning of this channel, a *concentration* profile at l' is a function that gives concentrations of all points in the channel along the line segment (of length w) that is perpendicular to the channel and directed counter-clockwise to the flow. We will be interested in how this profile evolves with time, that is with the value of l' increasing.
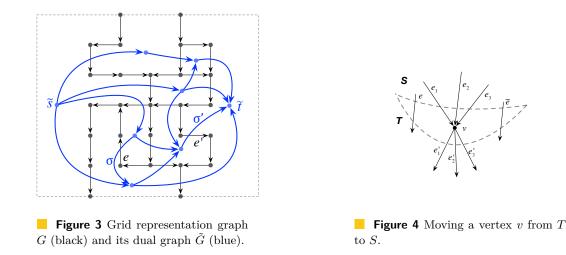
Figure 2 shows an example. Reactant and buffer are injected at the same rate into the top opening of a vertical straight channel, and allowed to mix while they flow. Initially the two fluids are separated, with the reactant to the left of the buffer, so the profile will be a 1/0 function. The flow is assumed to be laminar and the two fluids will gradually mix as a result of diffusion. After a period of time, this mixing produces a non-uniform concentration profile shown in Figure 2 on the right. This concentration profile is a smooth curve with the leftmost region having concentration 1, the rightmost region having concentration 0, and the middle region contains partially mixed fluids with concentration decreasing from left to right. Using the diffusion model, this profile function can be determined from the mixing time, which is the time it takes for the fluid to flow through the channel. Half of the width of this middle region is referred to as diffusion length and denoted L (normal to the flow direction, units m). It can be computed from the formula (see [10]):

$$L = 2\sqrt{Dt}. \tag{1}$$

where t is the mixing time and D is the diffusion coefficient of the fluid (units m^2/s).

In microfluidic grids, the flow may be repeatedly split or different flows may get combined, and the resulting concentration profile will not have the form in Figure 2 anymore; in fact, profile functions that arise in such grids are too complex to be captured analytically. Below we prove, however, that these profiles have a certain monotonicity property that will allow us to approximate them by a simpler function. Interestingly, this monotonicity property involves the concept of the partial order that is dual to the flow pattern.

Concentration monotonicity. The intuition behind the monotonicity property is illustrated in Figure 2; intuitively, the profile function in a channel should be monotonely decreasing from left to right. This property is trivial if we start with a 1/0 profile (with pure reactant to the left of pure buffer) at the top of a vertical channel and allow the fluid

Figure 3 Grid representation graph G (black) and its dual graph $\tilde{G}$ (blue).

Figure 4 Moving a vertex v from T to S.

to diffuse when it flows down along the channel. However, in a mixing grid the flow pattern may be quite complex. For example, depending on a grid's structure and flow velocities at its inlets, the flow direction in a vertical channel could be down or up. As a result, even the notions of "left" and "right" are not well defined anymore. Joins and splits complicate this issue even more. Thus, to define this monotonicity property, we need to capture the notion of "left-to-right direction" not only with respect to one channel, but also between different channels. This notion will be formalized using a partial ordering of the grid's channels. This partial order is defined as the dual order of the flow pattern in the grid. Below we formalize these concepts.

Once the flow directions are computed, the flow pattern through the grid design can be naturally represented as a straight-line planar drawing of a DAG (directed acyclic graph) whose nodes are grid points (including inlets and outlets) and edges are channels with directions determined by the flow. We will denote this graph by G.

Next, we construct a dual DAG $\tilde{G}$. To this end, enclose the grid in an axis-parallel rectangle, slightly wider than the grid, with the inlets on its top edge and outlets on its bottom edge, as in Figure 3. The grid (that is, the embedding of G) partitions this rectangle into regions. For each region of G, we create a vertex of $\tilde{G}$. Two vertices ϕ, ψ of $\tilde{G}$ are connected by an edge if the boundaries of their corresponding regions share at least one edge of G. The direction of the edge between ϕ and ψ is determined as follows: pick any edge (u, v) of G shared by the regions of ϕ and ψ. This edge (u, v) must have a different orientation in the boundaries of ϕ and ψ (clockwise in one and counter-clockwise in the other). Then the edge between ϕ and ψ is directed from the node where (u, v) is clockwise to the node where it is counter-clockwise. This definition does not depend on the choice of (u, v). We will refer to this edge as being dual to (u, v). It can be shown that $\tilde{G}$ is a DAG with a unique source $\tilde{s}$ and unique sink $\tilde{t}$ that correspond to the regions on the left and right of the grid design, respectively. (Except for secondary technical differences, the construction of such a dual can be found, for example, in [13, 2].)

We now use $\tilde{G}$ to define a partial order on the edges of G (that is, the channels of our grid design). Call two edges e, e' of G related in G if they are both on the same inlet-to-outlet path; otherwise call them *unrelated in G*. If e and e' are unrelated in G then, denoting by σ and σ' their dual edges, there must exist a path from $\tilde{s}$ to $\tilde{t}$ in $\tilde{G}$ that contains σ and σ'. If σ is before σ' on this path, then we write $e \trianglelefteq e'$, and say that e *dually precedes e'*. Figure 3 shows an example. It is not difficult to verify that relation "$\trianglelefteq$" is a partial order on G's

edges.

▶ **Theorem 1.** *(Concentration profile monotonicity.) Consider a grid design as described in Section 2 (in particular, the inlet concentrations are non-increasing) with some flow, and its corresponding graph G. The concentration profiles in G satisfy the following properties:*

(cpm1) For any edge e of G, each concentration profile across e is a non-increasing function.
(cpm2) For any two edges e, e' of G, if $e \trianglelefteq e'$ then each concentration value in each profile across e is at least as large as each concentration value in each profile across e'.

Proof. The formal proof of Theorem 1 is omitted here due to lack of space; we only give a brief sketch. For any two edges e, e' of G, we write $e \succcurlyeq e'$ to indicate that all concentration values in each profile across e are as large as all concentration values in each profile across e'. With this definition, part (cpm2) says that $e \trianglelefteq e'$ implies $e \succcurlyeq e'$.

Observe first that property (cpm1) is preserved as we move a profile along e in the flow direction, due to the properties of mixing (which shifts reactant mass from higher to lower values). With this in mind, it is sufficient to select, arbitrarily, one "representative" profile for each edge and to prove properties (cpm1) and (cpm2) only for these selected profiles.

Define a cut (S, T) of G in a natural way, as the partition of its vertices such that each inlet-to-outlet path visits vertices in S before visiting vertices in T. We prove by induction on $|S|$ that all edges with tail vertex in S satisfy the theorem. This is true in the base case, when S contains only inlets. In the inductive step, the definition of cuts implies that there is a vertex v that has all predecessors in S. Choose any such v. We move v from T to S (see Figure 4) and show that the inductive claim is preserved. The clockwise ordering of v's incoming edges $e_1, e_2, ...$ is the same as their $\trianglelefteq$ order. The same applies to the counter-clockwise order of its outgoing edges, $e'_1 \trianglelefteq e'_2 \trianglelefteq ...$. We also know that the concentration profile at v is the joined profile of $e_1, e_2, ...$ and then it is split into decreasing concentration profiles of $e'_1, e'_2, ...$. If there exist edges e and $\bar{e}$ in S that satisfy $e \trianglelefteq e_1 \trianglelefteq e_2 \trianglelefteq ... \trianglelefteq \bar{e}$, then e and $\bar{e}$ are also a predecessor and successor, respectively, of $e'_1, e'_2, ...$ in the $\trianglelefteq$ ordering. These observations and the inductive assumption applied to e and $\bar{e}$ imply that $e \succcurlyeq e'_1 \succcurlyeq e'_2 \succcurlyeq ... \succcurlyeq \bar{e}$. ◀

Approximate concentration profiles. In our technique, we approximate concentration profiles by simple 3-piece linear functions specified by four parameters a_L, a_R, d_L, and d_R, as shown in Figure 5. In interval $[0, d_L]$ the concentration is a_L, in interval $[w - d_R, w]$ the concentration is a_R, and the concentration linearly decreases in interval $[d_L, w - d_R]$, from a_L to a_R. Throughout the paper we will refer to such simplified profile functions as *SP-functions*. We have $w - d_L - d_R = 2L$, where L is the diffusion length value. The area under the profile curve, divided by the channel width w, represents the overall (average) concentration value of the fluid in this channel.

We remark that Theorem 1 remains valid for our approximate concentration profiles, instead of real ones. This is because its proof remains correct for any (not necessarily physically valid) mixing process that preserves the mass of reactant and buffer, and moves reactant mass rightward over time. Our approximate profile model has this property.

In Section 6 we explain how we can use SP-functions to compute approximate concentration profiles for each part of the grid design.

5   Computing Flow Rate and Pressure

The computation of the flow direction, flow rate and pressure in each channel of the grid is quite straightforward, and it can be achieved by solving a system of linear equations. The
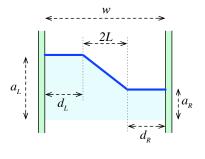
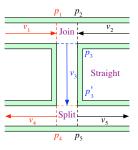**Figure 5** An SP-function profile.

Figure 6 Grid partition: a join node on the top, followed by a downward straight channel and then a split node.

unknowns are pressure values at every grid node and flow velocities in every channel. The first set of equations in this system are flow conservation equations: at every grid node the total inflow is equal to the total outflow. The second set of equations are Hagen-Poiseuille equations which give relationship between the flow rate and the pressure drop between the two ends of a channel: $\Delta P = QR$, where Q is the volumetric flow, and R is the flow resistance. As the resistance value is the same in every channel segment and the input data specifies the velocity at the grid inlets, the exact value for R is not needed and can be assumed to be 1.

One thing to note is that in our setting we assume there is no friction at the walls of the channel, thus implying that the velocity is uniform across the channel, which simplifies the formulas for updating the profiles. (With friction, the velocity profile is a parabolic function.) We found, however, that this assumption has only a negligible effect on the computed concentration values.

6   Algorithm for Estimating Concentration Profiles

The core of our algorithm is a procedure for updating approximate concentration profiles (represented by SP-functions) along the grid, namely part (4) of the overall algorithm in Section 3. We describe this procedure in this section.

As mentioned earlier in Section 3, the grid is partitioned into parts: straight channels and nodes, where nodes can be of several types depending on the flow directions of its channels: join nodes (2-way or 3-way), split nodes (2-way or 3-way), and combined join/split nodes (2 inflows and 2 outflows). This partitioning is illustrated in Figure 6. In this figure, the channels are cut at points p_1, p_2, p_3, p_3', p_4 and p_5, producing one join node, one straight channel, and one split node.

In the join node at the top, flows 1 and 2 are joined into flow 3. The concentration profile at point p_3 is computed by combining SP-functions at points p_1 and p_2, taking the velocity ratios into account. The combined function may not be an SP-function, and if so, we approximate it by an SP-function.

The straight channel stretches from the beginning of the channel at point p_3 to its end point p_3'. The approximate SP-function at point p_3' is computed from the SP-function at point p_3 using the diffusion formula. (To account for mixing in the grid nodes, instead of the original channel length l, the algorithm uses a slightly larger value $\tilde{l} = l + w/2$, with w is the width of the channel.)

In the split node at the bottom, we use the SP-function at point p_3' and the flow velocities
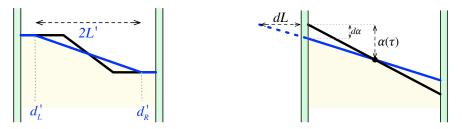
Figure 7 Updating the concentration profile in a straight channel in Case 1 (on the left) and Case 2 (on the right). The "before" profile is black and the "after" profile is blue.

to compute the split SP-functions at points p_4 and p_5. This case is relatively simple, as splitting an SP-function profile produces SP-functions, so no additional simplification is needed here.

6.1 Straight Channels

For a straight channel, the concentration profile changes over time with diffusion length increasing, that is with the middle portion of the SP-function becoming gradually longer and flatter. The SP-function may also change its form, with d_L becoming 0 or d_R becoming 0. We divide the evolution of the SP-function along a straight channel into time intervals short enough so that in each such time interval the profile function has the same form.

We now demonstrate how the SP-function changes in a straight channel during one of these time intervals. The fundamental idea behind our approach is this: Suppose that $d_L > 0$ and $d_R > 0$ in Figure **??** (Case 1 below). We then think of the current profile as being a result of mixing process in a straight channel (or for stationary fluid) that started from the original 1/0-valued profile and lasted for some unknown time t. This allows us to compute t from the diffusion length formula (1). Once we have t, we can compute the new SP-function at a time $t' = t + \Delta t$, where Δt is chosen to be the time until the next "event", which is the time when either the end of the channel is reached or when the profile form changes (that is, d_L or d_R becomes 0). This leads to a relatively simple solution for updating concentration profiles that satisfy $d_L > 0$ and $d_R > 0$, that is for SP-functions that have three non-empty segments. If $d_L = 0$ or $d_R = w$, or both, a slightly less direct approach is required (Cases 2, 3 and 4 below).

<u>Case 1</u>: $d_L > 0$ and $d_R > 0$ (see Figure 7). As explained above, using formula (1) we compute $t = L^2/4D$. Next, we compute the new diffusion length L' after time Δt: $L' = 2\sqrt{D(t + \Delta t)} = \sqrt{L^2 + 4D\Delta t}$. This will give us the new SP-function at time t', defined by parameters $d'_L = d_L - (L' - L)$ and $d'_R = d_R - (L' - L)$. We choose Δt to be the time until either the end of the channel is reached, or until one of d_L, d_R becomes 0, whichever happens first.

<u>Case 2</u>: $d_L = 0$ and $d_R = 0$ (see Figure 7). The channel boundaries introduce some distortion into the diffusion process that is difficult to model. Our approach here is based on the observation (verified experimentally) that this distortion has negligible effect on the overall profile. Thus, we think about the current concentration profile as the linearly decreasing part of the profile in a "virtual" wider channel in which the concentration profile has the same form as in Case 1, with $L = w/2 = 2\sqrt{Dt}$. The goal is to estimate the change of a_R and a_L in time interval $[t, t']$.
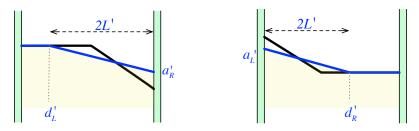
■ **Figure 8** Updating the concentration profile in a straight channel in Case 3 (on the left) and Case 4 (on the right). The "before" profile is black and the "after" profile is blue.

For $\tau \in [t, t']$, define $a_L(\tau)$ and $a_R(\tau)$ to be the concentrations at the left and right wall at time τ, and $\alpha(\tau) = (a_L(\tau) - a_R(\tau))/2$. We want to estimate the derivative $d\alpha/d\tau$.

To this end, let dL and $d\alpha$ denote the changes of L and $\alpha(\cdot)$ in a time interval $[\tau, \tau + d\tau]$, where $d\tau > 0$ is very small. (In the calculations below we will approximate some values assuming that $d\tau$ approaches 0.) We have $dL = 2\sqrt{D(\tau + d\tau)} - 2\sqrt{D\tau} = 2\sqrt{D}\, d\tau/(\sqrt{\tau + d\tau} + \sqrt{\tau}) \approx d\tau\,\sqrt{D/\tau}$, and, by simple geometry, $d\alpha = -\alpha(\tau)\, dL/(L + dL)$. Substituting, we get $d\alpha \approx -d\tau\,\alpha(\tau)/2\tau$. Thus the derivative is $d\alpha(\tau)/d\tau = -\alpha(\tau)/(2\tau)$.

Solving this differential equation and using the initial condition at t gives us $\alpha(\tau) = \alpha(t)\sqrt{t/\tau}$, where $\alpha(t) = (a_L - a_R)/2$. Thus, at time t' we have $\alpha(t') = \alpha(t)\sqrt{t/t'}$. From this we can calculate the new concentration values at the channel walls: $a'_L = a_L - \alpha(t)(1 - \sqrt{t/t'})$ and $a'_R = a_R + \alpha(t)(1 - \sqrt{t/t'})$. Here, t' is taken to be the time when the end of the channel is reached.

<u>Case 3</u>: $d_L > 0$ and $d_R = 0$ (see Figure 8). The new concentration profile in this case is computed based on the assumption that the value of d_L will decrease according to formula (1). This gives us the new value d'_L for the new SP-function, namely $d'_L = d_L - (L' - L)$ for $L' = 2\sqrt{D(t + \Delta t)} = \sqrt{4D\Delta t + (w - d_L)^2}$.

Then we use molecular preservation property (that is the area under the concentration profile does not change) and straightforward calculation to obtain the new concentration at the right wall, $a'_R = a_L - L(a_L - a_R)/L'$. Here, Δt is taken to be the time until either the end of the channel is reached or until d_L becomes 0, whichever happens first.

<u>Case 4</u>: $d_L = 0$ and $d_R > 0$ (see Figure 8). This case is symmetric to Case 3, and similar calculation gives us the values of d'_R and a'_L.

6.2   Joining Concentration Profiles.

To join flows, we first simply combine together the SP-functions of two or three joined channels, with the portion of the channel width that each joined flow occupies being proportional to the velocities of the inflows, as shown in Figure 9a. We will refer to this profile as the *combined profile*. In general, the combined profile will not be an SP-function. If this is the case, we will need to simplify it to an SP-function. This will be done in two steps. First we will convert the combined profile into a *tentative* SP-function (see Figure 9b), which will be later adjusted to satisfy the reactant volume preservation property.

The correctness of joining profiles depends critically on Theorem 1. This theorem implies that the concentration of the combined profile is non-increasing from left to right, as illustrated in Figure 9a. This figure shows two profiles being combined. The case of combining three profiles is essentially the same, as the middle channel's SP-function is only needed to
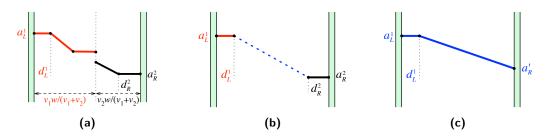
■ **Figure 9** Joinning concentration profiles of two flows (red and black). Combined profile (a). The tentative SP-function (b). (c) one possible final SP-function in the case when the area under the tentative profile is too small.

compute the area under the combined function; its parameters can be ignored. Thus, to simplify the description below, we will assume that we are dealing with a 2-way join node.

Let a_L^1 and d_L^1 represent the parameters of the combined profile inherited from the corresponding parameters of the left joined channel. (So a_L^1 is the concentration along the left wall in the left channel, and d_L^1 is the length of its SP-function's left flat segment, but rescaled according to the channel's flow velocity.) By a_R^2 and d_R^2 we denote the corresponding parameters inherited from the right joined channel. We take these four values as the parameters of our *tentative* SP-function profile. This function is only tentative, because the area under this SP-function may be different than that under the combined profile.

The final SP-function, whose parameters will be denoted a_L', d_L', a_R' and d_R', is computed from the tentative SP-function by adjusting its parameters to make sure that the reactant volume (the area under the profile) is preserved. This is done as follows. Let A be the area under the original combined profile (before converting it into the tentative form). If the area under the tentative profile is smaller than A, then the left segment of the final profile is the same as in the tentative profile, that is $a_L' = a_L^1$ and $d_L' = d_L^1$, while the middle and right segments are adjusted to increase the area to A: We start with $d_R' = d_R^2$ and $a_R' = a_R^2$. We then decrease d_R' until either the area equals A or d_R' is reduced to 0. If d_R' becomes 0, we then increase a_R' until the area becomes A. The case when the area under the tentative profile is larger than A is symmetric; in this case the right segment of the final profile is the same as in the tentative profile, and we gradually lower the middle and left segment to reduce the area to A.

6.3   Splitting Concentration Profiles

To split the flow at a node (either 2-way or 3-way), the split profiles are determined by dividing the profile of the inflow proportionally to the velocity ratios of the outflows (see Figure 10) and rescaling appropriately. For example, for two-way splits, if the velocities of the left and right outflows are v_1 and v_2, then the inflow profile is divided into two parts: the left one of width $v_1 w/(v_1 + v_2)$ and the right one of width $v_2 w/(v_1 + v_2)$. This produces two profiles which are then rescaled to have width w. Conveniently, splitting a profile represented by a SP-function produces profiles that are also in the same form, and the parameters of these new SP-functions can be determined with a straightforward computation, by rescaling. Thus, in this case no further simplifications of the new profiles are needed.
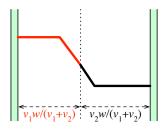
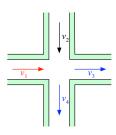**Figure 10** Splitting a profile into two profiles (red and black).

Figure 11 A join-and-split node. Flow v_1 and v_2 is joined and then split into v_3 and v_4.

6.4 Join-and-Split Nodes.

In the grid there may also be nodes with two inflows and two outflows. These nodes must have the form shown in Figure 11, namely the inflow channels are adjacent, and so are the outflow channels. (The other option, with the two inflows being opposite of each other, is impossible, as this would imply the existence of a flow circulation in the grid.)

We treat this case by reducing it to simple joins and splits, for which we provided solutions earlier. This is done by breaking the computation of the new profile into two sub-steps:

- First, we join the two inflow SP-functions, following the method described in Section 6.2.
- Then, we take the computed SP-function profile and split it into two SP-functions for the outflow channels, following the method discussed in Section 6.3.

7 Experimental Results

We used MATLAB® with COMSOL Multiphysics® via LiveLink™ [5] to generate our test grids. Note that in the method from [14], most generated chips have unreachable or "dead-end" channels, namely channels that do not appear on any inlet-to-outlet path. Such channels are redundant, as they have no effect on the mixing process. Our generator uses a similar approach as in [7] to generate only grids that are connected and have no redundant channels. Figure 12 shows four examples of random 12×12 grids obtained from our generator as well as their outlet concentrations.

Our concentration prediction algorithm is implemented in Python and tested on a 3.50GHz quad core 32GB RAM workstation. We conducted an experimental comparison of our algorithm with COMSOL simulation. In our experiment, we used 200 12×12 sample random grids (obtained from our generator) with two inlets (the left has reactant with concentration 1 and the right has buffer with concentration 0) and three outlets. The flow velocities at the inlets are both of constant rate 1 mm/s. The reactant is sodium, with diffusion coefficient value $1.33 \times 10^{-4} mm^2/s$. We used slower velocities than the chips of [14] in order to increase the time the fluid spends in the chip, which improves variability of concentration values at the outlets.

For COMSOL simulations we used very fine triangular meshes containing 5-10 millions elements. This mesh size was determined through a mesh refinement study to ensure that this setting does not affect outlet concentrations. For a random 12×12 grid we did a sweep on mesh element size by reducing the size at each step and observed the changes in outlet concentrations, repeating until the changes are less than 1% of maximum concentration.

The results for fluid velocities at the 3 outlets are very consistent with COMSOL simulation, with the average percentage difference of velocity values being 0.8%. For concentration
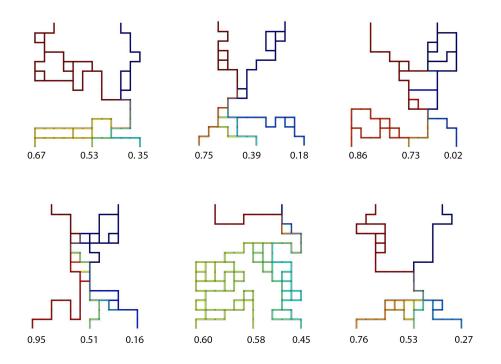
Figure 12 Randomly constructed 12×12 grids with concentration values at the outlets.

values at the outlets, the average absolute difference is 0.006 mol/m^3, which is 0.6% of the maximum concentration. The maximum absolute difference is 0.07 mol/m^3. Figure 13 shows the difference of concentration values at the 3 outlets between the algorithm and COMSOL, on 16 randomly selected grid designs.

Execution times are measured on the same sample set of 200 grids. On average, with our mesh setting, COMSOL takes approximately 21.3 minutes to finish the computation of one 12×12 grid. These times also vary significantly among different grids, with the fastest time of about 6 minutes and the longest around 30 minutes. Our algorithm is several orders of magnitude faster, requiring on average only 0.0075 second to process one grid. It also uses much less memory: the memory used for concentration profile computations is only linear in the side of the mixing grid design. COMSOL memory requirements are orders of magitude higher, as it depends on the size of the mesh used for the simulation.

We also performed an experiment to show that randomly generated 12×12 grid designs can produce a large collection of sufficiently different concentration vectors, and that a useful library of mixing grids can be successfully populated using our random grid generator and concentration prediction algorithm. We generated 50 million random designs on which we run our algorithm to compute output concentrations. We then filtered out grids that were redundant, in the sense that their output concentration values differed by no more than 0.01. The resulting grid library consisted of 2600 different concentration vectors.

8   Discussion

In this work we show that fluid mixing in microfluidic grids can be efficiently simulated using simple 3-piece linear functions to model concentration profiles. Our algorithm is very
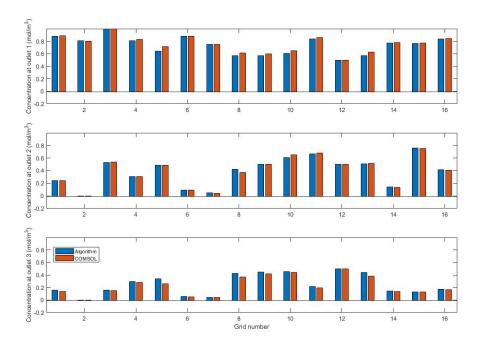
Figure 13 Comparison of concentration values at the outlets for sixteen randomly selected grids. Blue bars represent our algorithm and red bars represent COMSOL.

fast, outperforming COMSOL simulations by several orders of magnitude in term of running time, while producing nearly identical results.

While our current implementation of the algorithm assumes that the input is a grid design, the overall technique applies to arbitrary acyclic planar graphs. The only required assumptions involve inlets and outlets: all inlets and outlets must be located on the external face, cannot interleave, and the inlet concentrations must be non-decreasing in the clockwise direction along the external face. This is not a significant restriction, as in a microfluidic device its inlets and outlets would normally be located along its external boundary.

Another possible enhancement of our method is related to the assumption that the mixing process in microfluidic grids is exclusively caused by diffusion. This is a valid assumption for flows along straight channels, and it gives a good approximation of outlet concentrations for slow fluid velocity, typical for most microfluidic chips. Prior work in [1] showed, however, that with increased velocities, convection generated in channel bends affects mixing as well. (This will also likely apply to the split and join nodes.) Taking such convections effects into account could further improve the accuracy of our method.

------ **References** ------

1 Nobuaki Aoki, Ryota Umei, Atsufumi Yoshida, and Kazuhiro Mae. Design method for micromixers considering influence of channel confluence and bend on diffusion length. *Chem-*

ical Engineering Journal, 167(2-3):643–650, 2011.

2   Giuseppe Di Battista and Roberto Tamassia. Algorithms for plane representations of acyclic digraphs. *Theoretical Computer Science*, 61(2):175 – 198, 1988.

3   S. Bhattacharjee, B.B. Bhattacharya, and K. Chakrabarty. *Algorithms for Sample Preparation with Microfluidic Lab-on-Chip*. River Publishers Series in Biomedical Engineering. River Publishers, 2019.

4   S Bhattacharjee, S Poddar, S Roy, J Huang, and B Bhattacharya. Dilution and mixing algorithms for flow-based microfluidic biochips. *IEEE Transactions on Computer-Aided Design of Integrated Circuits and Systems*, 36(4):614–627, April 2017.

5   COMSOL, Inc. Comsol.

6   Stephen C. Jacobson, Timothy E. McKnight, and J. Michael Ramsey. Microfluidic devices for electrokinetically driven parallel and serial mixing. *Analytical Chemistry*, 71(20):4455–4459, 1999.

7   Weiqing Ji, Tsung-Yi Ho, and Hailong Yao. More effective randomly-designed microfluidics. *2018 IEEE Computer Society Annual Symposium on VLSI (ISVLSI)*, 2018.

8   Kim Jungkyu, Johnson Michael, Hill Parker, and Gale Bruce. Microfluidic sample preparation: cell lysis and nucleic acid purification. *Integrative Biology*, 1:574–586, Oct 2009.

9   Athina S. Kastania, Katerina Tsougeni, George Papadakis, Electra Gizeli, George Kokkoris, Angeliki Tserepi, and Evangelos Gogolides. Plasma micro-nanotextured polymeric micro-mixer for dna purification with high efficiency and dynamic range. *Analytica Chimica Acta*, 942:58–67, 2016.

10   Brian J. Kirby. *Micro- and nanoscale fluid mechanics: transport in microfluidic devices*. Cambridge University Press, 2013.

11   Brian M. Paegel, William H. Grover, Alison M. Skelley, Richard A. Mathies, and Gerald F. Joyce. Microfluidic serial dilution circuit. *Analytical Chemistry*, 78(21):7522–7527, 2006. PMID: 17073422.

12   Todd M. Squires and Stephen R. Quake. Microfluidics: Fluid physics at the nanoliter scale. *Rev. Mod. Phys.*, 77:977–1026, Oct 2005.

13   Roberto Tamassia and Ioannis G. Tollis. A unified approach to visibility representations of planar graphs. *Discrete & Computational Geometry*, 1(4):321–341, Dec 1986.

14   Junchao Wang, Philip Brisk, and William H. Grover. Random design of microfluidics. *Lab Chip*, 16:4212–4219, 2016.

15   Paul Yager, Thayne Edwards, Elain Fu, Kristen Helton, Kjell Nelson, Milton R. Tam, and Bernhard H. Weigl. Microfluidic diagnostic technologies for global public health. *Nature News*, Jul 2006.